THE JOURNAL OF PHYSICAL CHEMISTRY A
A JOURNAL OF THE AMERICAN CHEMICAL SOCIETY

pubs.acs.org/JPCA

Article

Electron Transfer under the Floquet Modulation in Donor–Bridge–Acceptor Systems

Yu Su, Zi-Hao Chen, Haojie Zhu, Yao Wang,* Lu Han, Rui-Xue Xu, and YiJing Yan*

Cite This: J. Phys. Chem. A 2022, 126, 4554–4561

Read Online

ACCESS | Metrics & More | Article Recommendations

ABSTRACT: Electron transfer (ET) processes are of broad interest in modern chemistry. With the advancements of experimental techniques, one may modulate the ET via such events as light–matter interactions. In this work, we study the ET under a Floquet modulation occurring in the donor–bridge–acceptor systems, with the rate kernels projected out from the exact dissipaton equation of motion formalism. This together with the Floquet theorem enables us to investigate the interplay between the intrinsic non-Markovianity and the driving periodicity. The observed rate kernel exhibits a Herzberg–Teller-like mechanism induced by the bridge fluctuation subject to effective modulation.

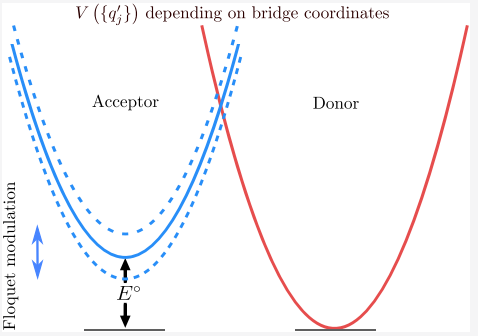

INTRODUCTION

Electron transfer (ET) processes are of broad interest in modern chemistry,[1−4] and many of them occur in the donor–bridge–acceptor (DBA) scenarios.[5−12] The bridge, which remains itself before and after the reaction, could be considered as a rigid spacer within an intramolecular ET system.[10] In condensed phases, the solvent environment also plays a crucial role.[13−17] Fluctuations of both the bridge and the solvent will manifestly affect the rate of ET processes. From a theoretical point of view, one can in principle exactly construct the generalized rate equation,

$$\dot{P}_{\rm D}(t) = -\int_0^t {\rm d}\tau k(t-\tau;\, t)P_{\rm D}(\tau) + \int_0^t {\rm d}\tau k'(t-\tau;\, t)P_{\rm A}(\tau) \tag{1}$$

Here, $P_{\rm D}(t)$ and $P_{\rm A}(t)$ are the donor and acceptor populations, respectively. The forward and backward rate memory kernels, $k(\tau;\, t)$ and $k'(\tau;\, t)$, have involved the influences of the bridge fluctuations, the solvent effects, and the possibly existent external modulations. Here, the variable τ characterizes the memory time scale, that is, the non-Markovianity, and t represents the time–dependence due to the external fields. The rate kernels are regularly computed and examined to study the memory effect in rate processes.[18−22]

With the advancements of experimental techniques, one can modulate the ET process via such events as light–matter interactions. Especially, if the external modulation is periodic, it is called the Floquet modulation.[23−27] In this work, we investigate how the ET rate kernels will be influenced by the fluctuating bridges and the Floquet modulation, with attention to the intrinsic non-Markovianity and the external periodicity. Specifically, we will focus on the case in which the energy difference between the donor state $|{\rm D}\rangle$ and the acceptor state $|{\rm A}\rangle$ is periodically modulated, which can be realized via the field–dipole interaction or the Stark effect.[26] We first give a perturbative analysis, followed by a discussion on the influences of the fluctuating bridge and the period of modulation. Then the non-Markovian rate kernels in eq 1 are projected out from the exact dissipaton equation of motion (DEOM).[28] This is the second quantization generation of the notable hierarchical equations of motion (HEOM) formalism,[29−34] covering both the reduced system and hybrid bath modes dynamics.[28,35−37] The linear space algebra of DEOM facilitates the utilization of Nakajima–Zwanzig projection operator technique, so that we can focus on any subspace dynamics and construct non-Markovian rate kernels.[19] The rate kernels are investigated with a DBA model system via both numerical and analytical methods in the DEOM framework. Especially, we pay attentions to the interplay between the intrinsic non-Markovianity and the driving periodicity, with the help of the Floquet theorem. The observed rate kernel exhibits a Herzberg–Teller-like mechanism induced by the bridge fluctuation subject to effective modulation. Throughout this

Received: May 12, 2022
Revised: June 13, 2022
Published: July 4, 2022

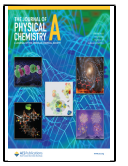

paper, we set $\hbar = 1$ and $\beta = 1/(k_B T)$ with k_B being the Boltzmann constant and T being the temperature.

THEORETICAL MODEL AND PERTURBATIVE ANALYSIS

Consider an ET DBA system with the total composite Hamiltonian,

$$H_{ET} = h_D|D\rangle\langle D| + (E^\circ + h_A)|A\rangle\langle A| + H_B + V(\{\tilde{q}_k\})(|D\rangle\langle A| + |A\rangle\langle D|) \quad (2)$$

Here $V(\{\tilde{q}_k\})$ depends on the bridge coordinates, and the fluctuating bridges Hamiltonian is $H_B = \sum_k \frac{\tilde{\omega}_k}{2}(\tilde{p}_k^2 + \tilde{q}_k^2)$. In eq 2, $E^\circ \simeq \Delta_r G^\circ$ amounts to the standard reaction Gibbs energy, for the electron transferring from $|D\rangle$ to $|A\rangle$. Donor and acceptor are both associated with their own solvent environments, h_D and h_A, where $h_D = \sum_j \frac{\omega_j}{2}(p_j^2 + x_j^2)$ and $h_A = \sum_j \frac{\omega_j}{2}[p_j^2 + (x_j - d_j)^2]$, respectively. The total ET composite was initially $\rho_T(t_0) = \rho^{eq}(T)\otimes|D\rangle\langle D|$, the thermal equilibrium in the donor state, with $\rho^{eq}(T) \equiv (e^{-\beta h_D}/\mathrm{tr}\, e^{-\beta h_D}) \otimes (e^{-\beta H_B}/\mathrm{tr}\, e^{-\beta H_B})$. Floquet modulation leads to the periodic changes of E°, as

$$E^\circ \to E(t) = E^\circ + \mathcal{E}\cos(\Omega t) \quad (3)$$

with the amplitude of $\mathcal{E}$ and the frequency of Ω. We sketch these theoretical settings in Figure 1.

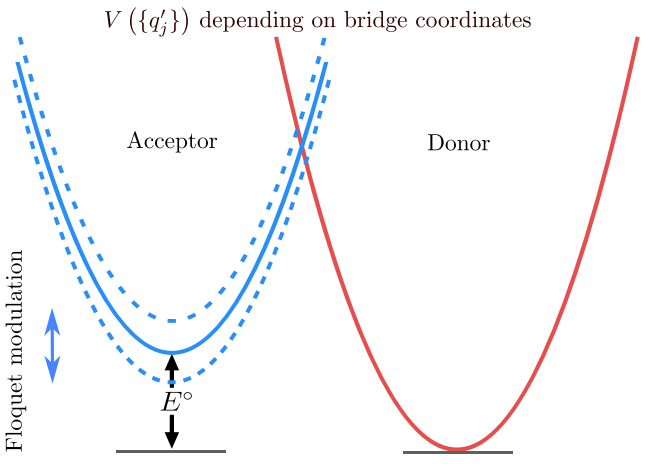

Figure 1. Schematics of ET under the Floquet modulation in the DBA system.

In the absence of modulation ($\mathcal{E} = 0$), the standard perturbation theory gives the forward rate constant the expression:[10,12]

$$K_0 = 2\,\mathrm{Re}\int_0^\infty \mathrm{d}t v(t)\, e^{-i(E^\circ+\lambda)t}\, e^{-g(t)} \quad (4a)$$

where $v(t) = \langle V(\{\tilde{q}_k(t)\})V(\{\tilde{q}_k\})\rangle_B$ with $\tilde{q}_k(t) \equiv e^{iH_B t}\tilde{q}_k\, e^{-iH_B t}$ and $\langle\cdot\rangle_B \equiv \mathrm{tr}(\cdot e^{-\beta H_B})/\mathrm{tr}\, e^{-\beta H_B}$. In eq 4a, $\lambda \equiv \langle\hat{U}\rangle_D \equiv \langle h_A - h_D\rangle_D$ and

$$g(t) = \int_0^t \mathrm{d}\tau \int_0^\tau \mathrm{d}\tau' C(\tau - \tau') \quad (4b)$$

where the correlation $C(t) \equiv \langle\delta\hat{U}(t)\delta\hat{U}\rangle_D$ with $\delta\hat{U} = \hat{U} - \lambda$ and $\delta\hat{U}(t) \equiv e^{ih_D t}\delta\hat{U}\, e^{-ih_D t}$.

In the presence of modulation ($\mathcal{E} \neq 0$), the time−dependent Hamiltonian $H_T(t)$ can be recast as

$$H_T(t) = H(t; \{\tilde{q}_k\}) + h_D + H_B - |A\rangle\langle A|\delta\hat{U} \quad (5a)$$

with

$$H(t; \{\tilde{q}_k\}) = (E^\circ + \mathcal{E}\cos\Omega t + \lambda)|A\rangle\langle A| + \hat{V} \quad (5b)$$

and

$$\hat{V} = V(\{\tilde{q}_k\})(|D\rangle\langle A| + |A\rangle\langle D|) \quad (5c)$$

To proceed, one may employ a unitary transformation generated by

$$\Lambda(t) \equiv e^{-i\varphi(t)|A\rangle\langle A|} \quad \text{with} \quad \varphi(t) = \mathcal{E}\sin(\Omega t)/\Omega \quad (6)$$

Under such a unitary transformation, we obtain the new Hamiltonian

$$H_T'(t) = \Lambda^\dagger(t)H_T(t)\Lambda(t) - i\Lambda^\dagger(t)\frac{\partial}{\partial t}\Lambda(t) = H'(t; \{\tilde{q}_k\}) + h_D + H_B - |A\rangle\langle A|\delta U \quad (7a)$$

where

$$H'(t; \{\tilde{q}_k\}) = (E^\circ + \lambda)|A\rangle\langle A| + \hat{V}'(t) \quad (7b)$$

with

$$\hat{V}'(t) = V(\{\tilde{q}_k\})(e^{-i\varphi(t)}|D\rangle\langle A| + e^{i\varphi(t)}|A\rangle\langle D|) \quad (7c)$$

It is easy to check, eq 5 generates the same population dynamics as eq 7. In the high-frequency limit, we could take the time average of $H_T'(t)$ over one period $T_0 \equiv 2\pi/\Omega$ to modify the rate constant given by perturbation theory [cf. eq 4a]. To this end, we do the approximation

$$H_T'(t) \to \tilde{H}_T \equiv \frac{1}{T_0}\int_0^{T_0} \mathrm{d}t H_T'(t)$$

and this amounts to

$$\hat{V}(t) \to \tilde{V} \equiv V(\{\tilde{q}_k\})J_0(\mathcal{E}/\Omega)$$

with $J_0(z)$ being the zeroth order Bessel function. Therefore, the nonadiabatic rate under the high−frequency Floquet modulation reads

$$K_0 = 2J_0^2(\mathcal{E}/\Omega)\mathrm{Re}\int_0^\infty \mathrm{d}t v(t)\, e^{-i(E^\circ+\lambda)t}\, e^{-g(t)} \quad (8)$$

This perturbative rate formula serves as a reference for the following nonperturbative exhibitions. For illustrations, we assume $V(\{\tilde{q}_k\})$ is in the form of[12]

$$V(\{\tilde{q}_k\}) \equiv \langle V\rangle_B - \delta\hat{V} = \langle V\rangle_B - \sum_k \tilde{c}_k\tilde{q}_k \quad (9)$$

This is intrinsically the Herzberg−Teller coupling scenarios that can be exactly handled by DEOM−space quantum mechanics.[38]

PROJECTED DEOM TO RATE KERNELS

To proceed we introduce

$$v(t) = \langle V\rangle_B^2 + \langle\delta\hat{V}(t)\delta\hat{V}\rangle_B = \langle V\rangle_B^2 + \sum_j \tilde{c}_j^2\langle\tilde{q}_j(t)\tilde{q}_j\rangle_B \quad (10)$$

https://doi.org/10.1021/acs.jpca.2c03308
J. Phys. Chem. A 2022, 126, 4554−4561

Now we can construct the DEOM based on eq 5, or equivalently eq 7: (i) In the former case, the system-plus-environment decomposition reads

$$H_T(t) = H_S(t) + h_E - |A\rangle\langle A|\delta\hat{U} - \hat{Q}\delta\hat{V} \tag{11}$$

where $h_E = h_D + H_B$,

$$H_S = (E^\circ + \mathcal{E}\cos\Omega t + \lambda)|A\rangle\langle A| + \langle V\rangle_B (|D\rangle\langle A| + |A\rangle\langle D|)$$

and $\hat{Q} = |D\rangle\langle A| + |A\rangle\langle D|$. In this case, the system Hamiltonian is time−dependent, while the dissipative mode $\hat{Q}$ is not; (ii) In the latter case,

$$H'_T(t) = H'_S(t) + h_E - |A\rangle\langle A|\delta\hat{U} - \hat{Q}'(t)\delta\hat{V} \tag{12}$$

Compared with eq 11, the $H'_S(t) = (E^\circ + \lambda)|A\rangle\langle A| + \langle V\rangle_B(e^{-i\varphi(t)}|D\rangle\langle A| + e^{i\varphi(t)}|A\rangle\langle D|)$ and $\hat{Q}'(t) = (e^{-i\varphi(t)}|D\rangle\langle A| + e^{i\varphi(t)}|A\rangle\langle D|)$ are different from the former case. Both the system Hamiltonian and the dissipative mode $\hat{Q}'(t)$ are time−dependent.

The rate kernels constructed from eq 11 should be exactly the same with that from eq 12, and our numerical results validate this point. The rate kernels are constructed via the DEOM approach. Based on the composite Hamiltonian in eq 11 or eq 12, we can write the DEOM in the form of

$$\dot{\boldsymbol{\rho}}(t) = -i\boldsymbol{\mathcal{L}}(t)\boldsymbol{\rho}(t) \tag{13}$$

This resembles $\dot{\rho}_T = -i\mathcal{L}_T(t)\rho_T$ with mapping the total system-plus-bath composite Liouvillian to the DEOM−space dynamics generator, $\mathcal{L}_T(t) \to \boldsymbol{\mathcal{L}}(t)$, and $\rho_T(t) \to \boldsymbol{\rho}(t) = \{\rho_{\mathbf{n}}^{(n)}(t); n = 0, 1, 2, \cdots\}$. Here, $\mathcal{L}_T(t) \equiv [H_T(t), \cdot]$ in case (i) or $[H'_T(t), \cdot]$ in case (ii). We will leave the detailed information on the DEOM (13) in the Appendix. To proceed, define DEOM−space projection operators, $\boldsymbol{\mathcal{P}}$ and $\boldsymbol{\mathcal{Q}} = \boldsymbol{\mathcal{I}} - \boldsymbol{\mathcal{P}}$, for partitioning $\boldsymbol{\rho} \equiv \{\rho_{\mathbf{n}}^{(n)}\}$ into the population and coherence components, respectively:[19]

$$\begin{aligned}\boldsymbol{\mathcal{P}}\boldsymbol{\rho}(t) &= \left\{\sum_a \rho_{aa}^{(0)}(t)|a\rangle\langle a|; 0, 0, \cdots\right\} \equiv \boldsymbol{p}(t)\\ \boldsymbol{\mathcal{Q}}\boldsymbol{\rho}(t) &= \left\{\sum_{a\neq b} \rho_{ab}^{(0)}(t)|a\rangle\langle b|; \rho_{\mathbf{n}}^{(n>0)}(t)\right\} \equiv \boldsymbol{\sigma}(t)\end{aligned} \tag{14}$$

We can now recast the DEOM 13 in terms of

$$\begin{bmatrix}\dot{\boldsymbol{p}}(t)\\ \dot{\boldsymbol{\sigma}}(t)\end{bmatrix} = -i\begin{bmatrix}\boldsymbol{\mathcal{P}}\boldsymbol{\mathcal{L}}(t)\boldsymbol{\mathcal{P}} & \boldsymbol{\mathcal{P}}\boldsymbol{\mathcal{L}}(t)\boldsymbol{\mathcal{Q}}\\ \boldsymbol{\mathcal{Q}}\boldsymbol{\mathcal{L}}(t)\boldsymbol{\mathcal{P}} & \boldsymbol{\mathcal{Q}}\boldsymbol{\mathcal{L}}(t)\boldsymbol{\mathcal{Q}}\end{bmatrix}\begin{bmatrix}\boldsymbol{p}(t)\\ \boldsymbol{\sigma}(t)\end{bmatrix} \tag{15}$$

After some simple algebra we obtain[19]

$$\dot{\boldsymbol{p}}(t) = \int_0^t d\tau\tilde{\boldsymbol{K}}(t-\tau; t)\boldsymbol{p}(\tau) \tag{16}$$

with the rate kernel being formally of

$$\tilde{\boldsymbol{K}}(t-\tau; t) = -\boldsymbol{\mathcal{P}}\boldsymbol{\mathcal{L}}(t)\boldsymbol{\mathcal{Q}}\boldsymbol{\mathcal{U}}(t, \tau)\boldsymbol{\mathcal{Q}}\boldsymbol{\mathcal{L}}(\tau)\boldsymbol{\mathcal{P}} \tag{17a}$$

with

$$\boldsymbol{\mathcal{U}}(t, \tau) \equiv \exp_+\left[-i\int_\tau^t d\tau'\boldsymbol{\mathcal{L}}(\tau')\right] \tag{17b}$$

Apparently, $-k(t-\tau; t)$ and $k'(t-\tau; t)$ in eq 1 are the $|D\rangle\langle D| \to |D\rangle\langle D|$ and $|A\rangle\langle A| \to |D\rangle\langle D|$ components of $\tilde{\boldsymbol{K}}(t-\tau; t)$, respectively.

RATE KERNEL ANALYSIS

In the following, we explicitly illustrate some key properties of the forward rate kernel $k(\tau; t)$ in eq 1, with the help of numerical examples. The analysis on $k'(\tau; t)$ is similar and thus omitted due to the limitation of space. It is worth noting the periodicity, $k(\tau; t) = k(\tau; t + T_0)$. The rigorous proofs are to be found in the Appendix. In Figure 2, we explicitly exhibit an

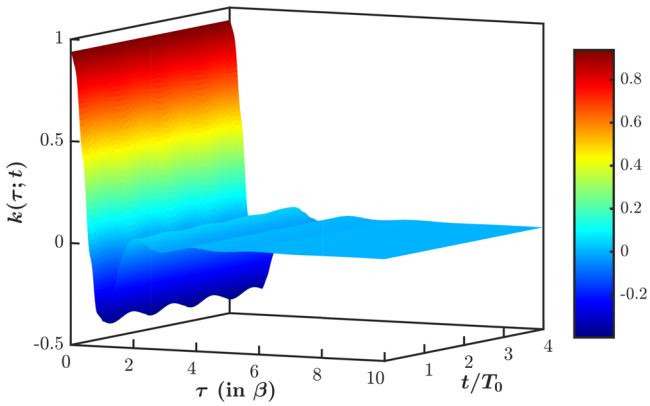

Figure 2. An example of rate kernel $k(\tau; t)$, in unit of β^{-2}. We adopt $\mathcal{E} = 2$, $E^\circ = 1.5$, and $\langle V\rangle_B = 0.2$ [cf. eq 11]. Besides, $\lambda = \lambda' = 0.2$ and $\gamma = \omega_0 = \zeta = 1$ [cf. eq 18]. All these parameters are in units of β^{-1}.

example of the computed rate kernels. The kernel $k(\tau; t)$ is plotted with respect to τ and t. The external modulation frequency adopts $\beta\Omega = 8\pi$. As shown in Figure 2, the kernel is periodic ($T_0 = 2\pi/\Omega$) with respect to t, and damping along the memory length, τ. In the simulations, we model the spectral densities, $J_D(\omega) \equiv 1/2\int_{-\infty}^{\infty}dt\, e^{i\omega t}\langle[\delta\hat{U}(t), \delta\hat{U}(0)]\rangle_D$ and $J_B(\omega) \equiv 1/2\int_{-\infty}^{\infty}dt\, e^{i\omega t}\langle[\delta\hat{V}(t), \delta\hat{V}(0)]\rangle_B$, as[39−41]

$$J_D(\omega) = \frac{2\lambda\gamma\omega}{\omega^2 + \gamma^2} \quad \text{and} \quad J_B(\omega) = \frac{2\lambda'\omega_0\zeta\omega}{(\omega^2 - \omega_0^2)^2 + \omega^2\zeta^2} \tag{18}$$

To further explicitly exhibit the underlying non-Markovianity, we represent the kernel in the frequency domain as

$$K(\omega; t) = \int_0^\infty d\tau k(\tau; t)\cos(\omega\tau) \tag{19}$$

Note the periodicity in t remains; that is, $K(\omega; t) = K(\omega; t + T_0)$. Figure 3 depicts the time-dependent frequency-resolved rate kernel, where this periodicity is manifest. Therefore, we may do the Fourier expansion with respect to t,

$$K(\omega; t) = \sum_{n=-\infty}^{\infty} K_n(\omega)\, e^{-in\Omega t} \tag{20a}$$

obtaining its components $\{K_n(\omega)\}$ being

$$K_n(\omega) = \frac{1}{T_0}\int_0^{T_0} dtK(\omega; t)\, e^{in\Omega t} \tag{20b}$$

In Figure 4, we plot the real parts of the Fourier components $\{K_n(\omega)\}$, exemplified with the same case as in Figure 2. These frequency−domain components exhibit the interplay between the external frequency, Ω, and the so−called Floquet

https://doi.org/10.1021/acs.jpca.2c03308
J. Phys. Chem. A 2022, 126, 4554−4561

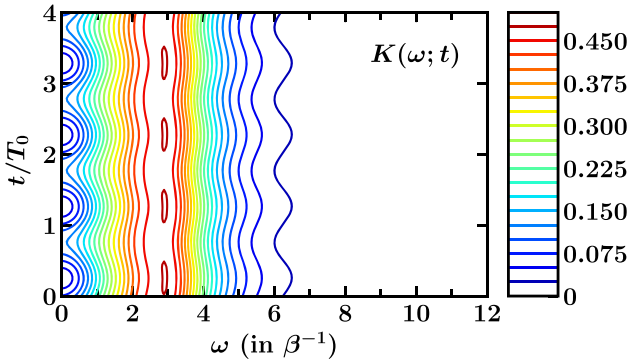

Figure 3. An example of $K(\omega; t)$, with the same parameters used in Figure 2.

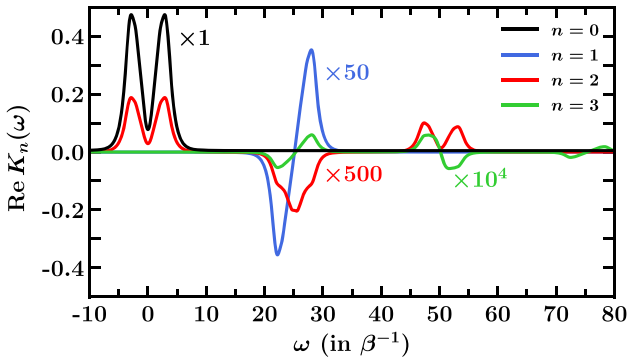

Figure 4. Real parts of the Fourier components $\{K_n(\omega)\}$ of the rate kernels in unit of β^{-1}, with the same parameters used in Figure 2.

frequency, ω_F. The ω_F is identified as the characteristic frequency of the Floquet Hamiltonian, H_T^F, defined via $e^{-iH_T^F T_0} \equiv \exp_+[-i\int_0^{T_0} dt\, H_T(t)]$. As shown in the figure, in the case of $\beta\Omega = 8\pi$ and $\beta\omega_F \sim 3$, the peaks of $\{K_n(\omega)\}$ are centered at the integer multiples of Ω. Meanwhile, each peak is split or deformed with split width being $2\omega_F$. With the help of the Floquet theorem, we may give an analytical explanation of this phenomenon, which is elaborated as follows.

We first recast eq 17a as

$$\tilde{\boldsymbol{K}}(\tau; t) = -\mathcal{P}\mathcal{L}(t)\mathcal{Q}\mathcal{U}(t, t-\tau)\mathcal{Q}\mathcal{L}(t-\tau)\mathcal{P}$$

Then, according to the Floquet theorem, the total propagator can be decomposed as[25]

$$U_T(t, 0) \equiv T_+ e^{-i\int_0^t d\tau H_T(\tau)} = e^{-iK_T^F(t)} e^{-iH_T^F t} \tag{21}$$

Here, the Floquet Hamiltonian, H_T^F, and stroboscopic kick operator, $K_T^F(t)$, are defined as

$$e^{-iH_T^F T_0} \equiv U(T_0, 0) \quad \text{and} \quad e^{-iK_T^F(t)} \equiv U(t, 0)\, e^{iH_T^F t} \tag{22}$$

respectively, where the stroboscopic kick operator satisfies $K_T^F(0) = K_T^F(nT_0) = 0$. Therefore, we immediately obtain in the DEOM−space that

$$\tilde{\boldsymbol{K}}(\tau; t) = -\mathcal{P}\mathcal{L}(t)\mathcal{Q}\mathcal{U}_K(t)\mathcal{G}_F(\tau)\mathcal{U}_K^\dagger(t-\tau)\mathcal{Q}\mathcal{L}(t-\tau)\mathcal{P} \tag{23}$$

with $\mathcal{G}_F(\tau)$, $\mathcal{U}_K(\tau)$, and $\mathcal{U}_K^\dagger(t-\tau)$ being $\exp\{-i\tau[H_T^F, \cdot]\}$, $\exp\{-i[K_T^F(\tau), \cdot]\}$ and $\exp\{i[K_T^F(t-\tau), \cdot]\}$ mapped into the DEOM space, respectively. Since the system is driven periodically, we can expand the rate kernel as

$$\tilde{\boldsymbol{K}}(\tau; t) = \sum_{n=-\infty}^{\infty}\sum_{m=-\infty}^{\infty} \mathcal{A}_n\mathcal{G}_F(\tau)\mathcal{B}_m\, e^{-i(n+m)\Omega t}\, e^{im\Omega\tau} \tag{24a}$$

where $\mathcal{A}_n \equiv -\frac{i}{T_0}\int_0^{T_0} dt\mathcal{P}\mathcal{L}(t)\mathcal{Q}\mathcal{U}_K(t)\, e^{in\Omega t}$ and

$$\mathcal{B}_m \equiv -\frac{i}{T_0}\int_0^{T_0} dt\mathcal{U}_K^\dagger(t)\mathcal{Q}\mathcal{L}(t)\mathcal{P}e^{im\Omega t}$$

By changing the summation indices, we obtain

$$\tilde{\boldsymbol{K}}(\tau; t) = \sum_{n=-\infty}^{\infty} e^{-in\Omega t}\sum_{m=-\infty}^{\infty} \mathcal{A}_{n-m}\mathcal{G}_F(\tau)\mathcal{B}_n\, e^{im\Omega\tau} \tag{24b}$$

and therefore the corresponding Fourier components in frequency domain are given by

$$\bar{\boldsymbol{K}}_n(\omega) = \int_0^\infty d\tau \sum_{m=-\infty}^{\infty} \mathcal{A}_{n-m}\mathcal{G}_F(\tau)\mathcal{B}_m\, e^{im\Omega\tau}\cos(\omega\tau) \tag{25}$$

Since the Floquet Hamiltonian is independent of time, one could express the Fourier components formally via the eigenstates of $\mathcal{L}_F$, the mapping of $[H_T^F, \cdot]$ in DEOM−space, as

$$\bar{\boldsymbol{K}}_n(\omega) = \int_0^\infty d\tau \sum_{m=-\infty}^{\infty}\sum_{\omega_F} \mathcal{A}_{n-m}(\omega_F) \mathcal{B}_m(\omega_F)\, e^{i(m\Omega-\omega_F)\tau}\cos(\omega\tau) \tag{26}$$

That is to say, we set $\mathcal{B}_m = \sum_{\omega_F}\mathcal{B}_m(\omega_F)$, such that $\mathcal{A}_{n-m}\mathcal{L}_F\mathcal{B}_m(\omega_F) = \omega_F\mathcal{A}_{n-m}(\omega_F)\mathcal{B}_m(\omega_F)$. In eq 26, the integral over τ gives the basic profile of peaks (real parts), proportional to

$$\alpha\left[\frac{1}{\omega - (m\Omega - \omega_F)} - \frac{1}{\omega + (m\Omega - \omega_F)}\right] + \alpha'\left[\frac{1}{\omega - (m\Omega + \omega_F)} - \frac{1}{\omega + (m\Omega + \omega_F)}\right] \tag{27}$$

with α and α' being the coefficients. Equation 27 thus explains the peak-split phenomenon in $\{K_n(\omega)\}$, the $|D\rangle\langle D| \to |D\rangle\langle D|$ components of $\{\bar{\boldsymbol{K}}_n(\omega)\}$.

HERZBERG−TELLER-LIKE MECHANISM

To conclude the paper, we remark on the Herzberg−Teller-like mechanism induced by the bridge fluctuation subject to effective modulation. In the absorption spectroscopy, the Herzberg−Teller mechanism manifests the non-Condon vibronic couplings, where the transition dipole moment involves the nuclear coordinate dependence. There exists a similar mechanism in our setting of ET with a fluctuating bridge. To illustrate this point, we first evaluate the Fourier components with or without bridge fluctuations. As shown in Figure 5, it is evident that the existence of a fluctuating bridge would broaden, strengthen, and deform each peak of the Fourier components. This reflects the Herzberg−Teller-like mechanism, as analyzed below. In the high-frequency limit $\varphi(t) \ll 1$, the Hamiltonian in eq 12 can be written in the form of

$$H_T'(t) = H_S^0 + h_E - |A\rangle\langle A|\delta\hat{U} - \hat{Q}\delta\hat{V} - \hat{\mu}_T^-\tilde{E}^+(t) - \hat{\mu}_T^+\tilde{E}^-(t) \tag{28}$$

https://doi.org/10.1021/acs.jpca.2c03308
J. Phys. Chem. A 2022, 126, 4554−4561

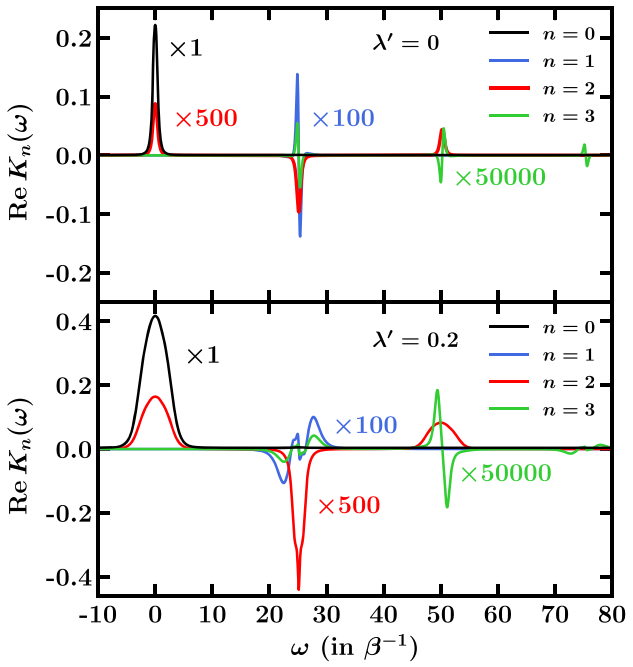

Figure 5. Real parts of the Fourier components evaluated with or without bridge fluctuation, in unit of β^{-1}. We set $\mathcal{E} = 0.2$, $\Omega = 8\pi$, $E^\circ = -0.2$, $\langle V\rangle_B = 0.2$, $\lambda = 0.2$, $\gamma = \omega_0 = \zeta = 1$ for both the cases, while λ' = 0 and 0.2 in the upper and lower panel, respectively.

with $H_S^0 = (E^\circ + \lambda)|A\rangle\langle A| + \langle V\rangle_B(|D\rangle\langle A| + |A\rangle\langle D|)$, $\hat{\mu}_T^+ = |A\rangle\langle D|(\langle V\rangle_B - \delta\hat{V}) = (\hat{\mu}_T^-)^\dagger$ and $\tilde{E}^+(t) = i\varphi(t) = [\tilde{E}^-(t)]^\dagger$. The last two terms in eq 28 can be seen as an effective dipole−field coupling, where the total dipole involves the bridge degrees of freedom. In the Markovian and high-frequency limits, the rate constant is given by

$$\check{K}_0 = K_0(\omega = 0) \tag{29}$$

which shall be compared with the perturbative result in eq 8. In Figure 6, we plot the rate constants K_0 and $\check{K}_0$ versus E°, with different strengths of bridge fluctuation. As shown in Figure 6, in the regime of $E^\circ + \lambda \sim 0$, the perturbative results with larger λ' depart more from the nonperturbative results.

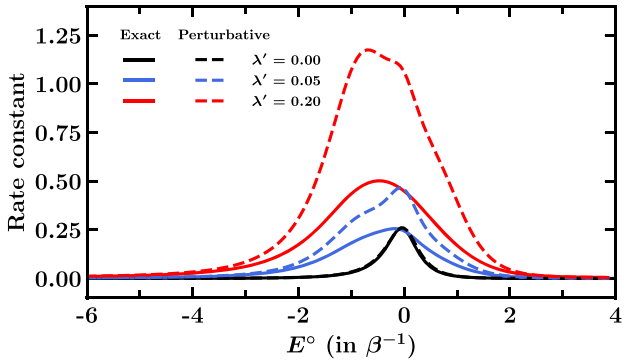

Figure 6. Rate constants K_0 and $\check{K}_0$ versus E° in unit of β^{-1}, with different strengths of bridge fluctuation, λ'. Other parameters are the same with that in Figure 5.

SUMMARY

We study the ET under the Floquet modulation occurring in the DBA systems. The rate kernels are constructed and evaluated via the exact projected dissipaton equation of motion formalism. This enables us to investigate the interplay between the intrinsic non-Markovianity and driving periodicity. The bridge fluctuations manifestly affect the rate kernel, exhibiting a Herzberg−Teller-like mechanism subject to effective modulation. It is anticipated that our study will benefit the design of ET manipulation in molecular systems. Besides, our analysis on rate kernels can be generalized to other physical chemistry processes when the involved memory effects can not be ignored, such as excitation energy transfer in light harvest systems.[26] For these systems, the Floquet modulation plays the role as a method to detect the intrinsic non-Markovianity of target systems, which shall serve as an auxiliary route to other detection methods. To illustrate this point, we give an example of the rate kernel under different modulations in the Appendix.

A BRIEF INTRODUCTION TO DEOM

Consider an arbitrary system coupled to the environment with the temperature T. Generally, the composite Hamiltonian can be decomposed into the system, the system−environment coupling, and the environment parts as

$$H_T(t) = H_s(t) + \sum_a \hat{Q}_a(t)\hat{F}_a + h_B \tag{30}$$

Here, the dissipative modes $\{\hat{Q}_a\}$ are rather arbitrary, while the environment Hamiltonian are adopted to be Gaussian. This requires not only that the h_B be harmonic but also that the hybrid reservoir modes $\{\hat{F}_a\}$ be linear. That is

$$h_B = \frac{1}{2}\sum_j \omega_j(p_j^2 + x_j^2) \quad \text{and} \quad \hat{F}_a = \sum_j c_{aj}x_j \tag{31}$$

Here, the oscillators of frequency $\{\omega_j\}$, with position $\{x_j\}$ and momentum $\{p_j\}$, are coupled to the system with strength $\{c_{aj}\}$. It can be seen that eq 30 with eq 31 covers both the Hamiltonians given by eqs 11 and 12.

For the Gaussian environment (also named as "bath"), its influences on the system is totally characterized by the spectral density, $J_{ab}(\omega) = \pi/2\sum_j c_{aj}c_{bj}\delta(\omega - \omega_j)$ for $\omega \geq 0$, and it is related to the statistical bath correlation via the fluctuation−dissipation theorem as[39,41]

$$\langle\hat{F}_a(t)\hat{F}_b(0)\rangle_B = \frac{1}{\pi}\int_{-\infty}^{\infty} d\omega \frac{e^{-i\omega t}J_{ab}(\omega)}{1 - e^{-\beta\omega}} \simeq \sum_{k=1}^{K}\eta_{abk}\, e^{-\gamma_k t} \tag{32}$$

Here, $\hat{F}_a(t) \equiv e^{ih_B t}\hat{F}_a e^{-ih_B t}$ is the hybrid bath operator in the h_B-interaction picture. The average $\langle\hat{O}\rangle_B \equiv \mathrm{tr}_B(\hat{O}\, e^{-\beta h_B})/\mathrm{tr}_B(e^{-\beta h_B})$ runs over the bare-bath thermal equilibrium ensembles for any operator $\hat{O}$. The multiexponential decomposition in the last identity can be readily achieved with some advancing sum-overpole schemes.[42,43] The exponents from the poles of Bose function and the corresponding pre-exponents coefficients are both real. On the other hand, those originating from the spectral density are either real or complex conjugate paired. Therefore, we can define $\bar{k}$ such that $\gamma_{\bar{k}} = \gamma_k^*$.

Dynamical variables in DEOM are the dissipaton-augmented-reduced density operators (DDOs):[28,36,44] $\rho_{\mathbf{n}}^{(n)}(t)$

https://doi.org/10.1021/acs.jpca.2c03308
J. Phys. Chem. A 2022, 126, 4554−4561

$\equiv \mathrm{tr}_B[(\prod_{ak} \hat{f}_{ak}^{n_{ak}})^\circ \rho_T(t)]$. Here, $\mathbf{n} \equiv \{n_{ak}\}$ specifies the configuration of the total n-dissipatons, where $n = \sum_{ak} n_{ak}$, with $n_{ak} \geq 0$ for bosonic dissipatons. The reduced system density operator is just $\rho_{\mathbf{0}}^{(0)}(t)$. The DEOM reads[28]

$$\begin{aligned}\dot{\rho}_{\mathbf{n}}^{(n)} =& -[H_S(t), \rho_{\mathbf{n}}^{(n)}] - \sum_{ak} n_{ak}\gamma_k \rho_{\mathbf{n}}^{(n)} \\ & - i\sum_{ak}[\hat{Q}_a(t), \rho_{\mathbf{n}_{ak}^+}^{(n+1)}] \\ & - i\sum_{abk} n_{ak}[\eta_{abk}\hat{Q}_a(t)\rho_{\mathbf{n}_{bk}^-}^{(n-1)} - \eta_{ab\bar{k}}^*\rho_{\mathbf{n}_{bk}^-}^{(n-1)}\hat{Q}_a(t)]\end{aligned} \tag{33}$$

This describes the same dynamics of the HEOM formalism.[29−33,45] It is worth emphasizing that the DEOM theory contains not only the above hierarchical dynamics, but also the dissipaton algebra.[37] For brevity, we could express eq 33 in the form of eq 13, resembling the traditional Liouville equation in which the total system-plus-bath composite Liouvillian is mapped to the DEOM−space dynamics generator.

PROOF OF THE PERIODICITY OF RATE KERNELS

Within the setting of periodicity, that is, $\mathcal{L}(t + T_0) = \mathcal{L}(t)$, one could obtain

$$\begin{aligned}\tilde{\boldsymbol{K}}(t-\tau; t+T_0) \equiv& -\mathcal{P}\mathcal{L}(t+T_0)\mathcal{Q}\mathcal{U}(t+T_0, \tau+T_0) \\ & \mathcal{Q}\mathcal{L}(\tau+T_0)\mathcal{P} \\ =& \mathcal{P}\mathcal{L}(t)\mathcal{Q}\mathcal{U}(t,\tau)\mathcal{Q}\mathcal{L}(\tau)\mathcal{P} \\ =& \tilde{\boldsymbol{K}}(t-\tau; t)\end{aligned} \tag{34}$$

Here we have used

$$\begin{aligned}&\mathcal{U}(t+T_0, \tau+T_0) \\ &= \exp_+\left[-i\int_{\tau+T_0}^{t+T_0} d\tau' \mathcal{L}(\tau')\right] \\ &= \exp_+\left[-i\int_{\tau}^{t} d\tau' \mathcal{L}(\tau'+T_0)\right] \\ &= \exp_+\left[-i\int_{\tau}^{t} d\tau' \mathcal{L}(\tau')\right] \\ &= \mathcal{U}(t,\tau)\end{aligned} \tag{35}$$

Therefore, we conclude $k(t-\tau; t)$ and $k'(t-\tau; t)$ are periodic with respect to their second parameters.

COMMENTS ON THE DETAILED BALANCE RELATION

In this appendix, we discuss the detailed balance relation of rate constants. In the Markovian limit, the rate equation reads

$$\dot{P}_D(t) = -K(\omega=0; t)P_D(t) + K'(\omega=0; t)P_A(t) \tag{36}$$

According to eq 20, we know that

$$\begin{aligned}K(0; t) =& \sum_{n=-\infty}^{\infty} K_n(0)\, e^{-in\Omega t} \quad \text{and} \\ K'(0; t) =& \sum_{n=-\infty}^{\infty} K_n'(0)\, e^{-in\Omega t}\end{aligned} \tag{37}$$

Substitute eq 37 into eq 36, and we obtain

$$\begin{aligned}\dot{P}_D(t) =& -\sum_{n=-\infty}^{\infty} K_n(0)\, e^{-in\Omega t}P_D(t) \\ & + \sum_{n=-\infty}^{\infty} K_n'(0)\, e^{-in\Omega t}P_A(t)\end{aligned} \tag{38}$$

In the high-frequency limits, the rate constant is given by $\check{K}_0 = K_0(0)$ and $\check{K}_0' = K_0'(0)$, and this leads to

$$\dot{P}_A(t) = -\dot{P}_D(t) \approx \check{K}_0 P_D(t) - \check{K}_0' P_A(t) \tag{39}$$

Define $P_{D/A}(z) \equiv \int_0^\infty dt\, e^{izt}P_{D/A}(t)$ with $\epsilon \equiv \mathrm{Im}z > 0$, and we can then recast eq 39 as

$$-izP_A(z) = \check{K}_0 P_D(z) - \check{K}_0' P_A(z) \tag{40}$$

where we have used $P_A(t=0) = 0$. Equation 40 then gives the detailed balance relation (setting $z = 0 + i\epsilon$)

$$(\check{K}_0' + \epsilon)/\check{K}_0 = P_D(z = i\epsilon)/P_A(z = i\epsilon) \tag{41}$$

Here, $P_{D/A}(t)$ shall be obtained from the DEOM calculations in the Markovian and high-frequency regime.

MORE ON THE RATE KERNEL UNDER MODULATIONS

In this appendix, we give an example of the rate kernel under different modulation frequencies.

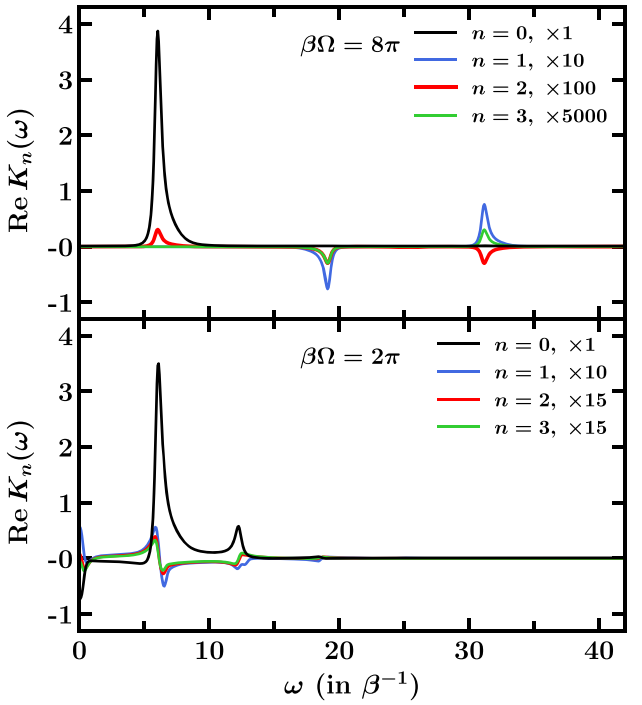

Figure 7. Example of the rate kernel under different modulation frequencies. We adopt $E^\circ = 6$, $\langle V\rangle_B = 1$ and $\lambda' = 0.05$ (in β^{-1}). Other parameters are the same with that in Figure 2 of the main text.

Results are shown in Figure 7. In this example, the Floquet frequency $\beta\omega_F \sim 2\pi$. The lower panel exhibits a resonance scenario. Compared with the upper panel with $\beta\Omega = 8\pi$, the resonance case exhibits some different characteristics. First, we observe the rate constant $\check{K}_0$, the $n = 0$ component of the kernel at $\omega = 0$, largely increases in this scenario, while it almost vanishes in the upper panel. Second, in the upper panel

https://doi.org/10.1021/acs.jpca.2c03308
J. Phys. Chem. A 2022, 126, 4554−4561

the $n = 0$ component is localized near $\omega = 2\pi$ while it is broadened in the lower panel. The localization in frequency domain implies a certain time length of memory, which may also be evidenced by such as two-dimensional spectroscopy techniques. Third, the $n > 0$ components shrink in the frequency domain, which implies the low-frequency effect becomes more manifest in resonance scenarios.

AUTHOR INFORMATION

Corresponding Authors

Yao Wang − *Department of Chemical Physics, University of Science and Technology of China, Hefei, Anhui 230026, China*; orcid.org/0000-0003-2939-208X; Email: wy2010@ustc.edu.cn

YiJing Yan − *Department of Chemical Physics, University of Science and Technology of China, Hefei, Anhui 230026, China*; Email: yanyj@ustc.edu.cn

Authors

Yu Su − *Department of Chemical Physics, University of Science and Technology of China, Hefei, Anhui 230026, China*

Zi-Hao Chen − *Department of Chemical Physics, University of Science and Technology of China, Hefei, Anhui 230026, China*

Haojie Zhu − *Department of Chemical Physics, University of Science and Technology of China, Hefei, Anhui 230026, China*

Lu Han − *Department of Chemical Physics, University of Science and Technology of China, Hefei, Anhui 230026, China*

Rui-Xue Xu − *Department of Chemical Physics, University of Science and Technology of China, Hefei, Anhui 230026, China*

Complete contact information is available at: https://pubs.acs.org/10.1021/acs.jpca.2c03308

Notes

The authors declare no competing financial interest.

ACKNOWLEDGMENTS

The authors thank the Ministry of Science and Technology of China (Grant No. 2021YFA1200103) and the National Natural Science Foundation of China (Grant Nos. 22103073, 22173088 and 21903078) for support. Y.S. and H.J.Z. thank also the College Students' Innovative Entrepreneurial Training Plan Program (2020) for partial support. Y.W. and Z.H.C. thank also the GHfund B (20210702) for partial support.

REFERENCES

(1) Marcus, R. A. On the energy of oxidation-reduction reactions involving electron transfer. I. *J. Chem. Phys.* **1956**, *24*, 966−978.

(2) Marcus, R. A. Chemical and electrochemical electron-transfer theory. *Annu. Rev. Phys. Chem.* **1964**, *15*, 155.

(3) Sumi, H.; Marcus, R. A. Dynamics effects in electron-transfer reactions. *J. Chem. Phys.* **1986**, *84*, 4894−4914.

(4) Marcus, R. A. Electron transfer reactions in chemistry: Theory and experiment. *Rev. Mod. Phys.* **1993**, *65*, 599.

(5) Delor, M.; Scattergood, P. A.; Sazanovich, I. V.; Parker, A. W.; Greetham, G. M.; Meijer, A. J. H. M.; Towrie, M.; Weinstein, J. A. Toward control of electron transfer in donor-acceptor molecules by bond-specific infrared excitation. *Science* **2014**, *346*, 1492−1495.

(6) Bixon, M.; Jortner, J. Electron transfer-from isolated molecules to biomolecules. *Adv. Chem. Phys.* **1999**, *106*, 35−208.

(7) Newton, M. D. *Electron Transfer in Chemistry*; John Wiley & Sons, Ltd, 2001; Chapter 1, pp 2−63.

(8) Skourtis, S. S.; Beratan, D. N. *Electron Transfer in Chemistry*; John Wiley & Sons, Ltd, 2001; Chapter 3, pp 109−125.

(9) Nitzan, A. Electron transmission through molecules and molecular interfaces. *Annu. Rev. Phys. Chem.* **2001**, *52*, 681−750.

(10) Troisi, A.; Nitzan, A.; Ratner, M. A. A rate constant expression for charge transfer through fluctuating bridges. *J. Chem. Phys.* **2003**, *119*, 5782−5788.

(11) Galperin, M.; Ratner, M. A.; Nitzan, A. Molecular transport junctions: Vibrational effects. *J. Phys.: Condens. Matter* **2007**, *19*, 103201.

(12) Zhao, Y.; Liang, W. Non-Condon nature of fluctuating bridges on nonadiabatic electron transfer: Analytical interpretation. *J. Chem. Phys.* **2009**, *130*, 034111.

(13) Wolynes, P. G. Dissipation, tunneling, and adiabaticity criteria for curve crossing problems in the condensed phase. *J. Chem. Phys.* **1987**, *86*, 1957−66.

(14) Sparpaglione, M.; Mukamel, S. Adiabatic vs. nonadiabatic electron transfer and longitudinal solvent dielectric relaxation: Beyond the Debye model. *J. Phys. Chem.* **1987**, *91*, 3938−43.

(15) Sparpaglione, M.; Mukamel, S. Dielectric friction and the transition from adiabatic to nonadiabatic electron transfer. I. Solvation dynamics in Liouville space. *J. Chem. Phys.* **1988**, *88*, 3263.

(16) Sparpaglione, M.; Mukamel, S. Dielectric friction and the transition from adiabatic to nonadiabatic electron transfer in condensed phases. II Application to non-Debye solvents. *J. Chem. Phys.* **1988**, *88*, 4300.

(17) Han, P.; Xu, R. X.; Li, B. Q.; Xu, J.; Cui, P.; Mo, Y.; Yan, Y. J. Kinetics and thermodynamics of electron transfer in Debye solvents: An analytical and nonperturbative reduced density matrix theory. *J. Phys. Chem. B* **2006**, *110*, 11438−43.

(18) Gong, Z. H.; Tang, Z. F.; Mukamel, S.; Cao, J. S.; Wu, J. L. A continued fraction resummation form of bath relaxation effect in the spin-boson model. *J. Chem. Phys.* **2015**, *142*, 084103.

(19) Zhang, H. D.; Yan, Y. J. Kinetic rate kernels via hierarchical Liouville-space projection operator approach. *J. Phys. Chem. A* **2016**, *120*, 3241−3245. Special Issue: Ronnie Kosloff Festschrift.

(20) Xu, M.; Yan, Y.; Liu, Y.; Shi, Q. Convergence of high order memory kernels in the Nakajima-Zwanzig generalized master equation and rate constants: Case study of the spin-boson model. *J. Chem. Phys.* **2018**, *148*, 164101.

(21) Yan, Y.; Xu, M.; Liu, Y.; Shi, Q. Theoretical study of charge carrier transport in organic molecular crystals using the Nakajima-Zwanzig-Mori generalized master equation. *J. Chem. Phys.* **2019**, *150*, 234101.

(22) Dan, X.; Xu, M.; Yan, Y.; Shi, Q. Generalized master equation for charge transport in a molecular junction: Exact memory kernels and their high order expansion. *J. Chem. Phys.* **2022**, *156*, 134114.

(23) Bukov, M.; D'Alessio, L.; Polkovnikov, A. Universal high-frequency behavior of periodically driven systems: from dynamical stabilization to Floquet engineering. *Adv. Phys.* **2015**, *64*, 139−226.

(24) Mikami, T.; Kitamura, S.; Yasuda, K.; Tsuji, N.; Oka, T.; Aoki, H. Brillouin-Wigner theory for high-frequency expansion in periodically driven systems: Application to Floquet topological insulators. *Phys. Rev. B* **2016**, *93*, 144307.

(25) Restrepo, S.; Cerrillo, J.; Bastidas, V. M.; Angelakis, D. G.; Brandes, T. Driven Open Quantum Systems and Floquet Stroboscopic Dynamics. *Phys. Rev. Lett.* **2016**, *117*, 250401.

(26) Thanh Phuc, N.; Ishizaki, A. Control of Excitation Energy Transfer in Condensed Phase Molecular Systems by Floquet Engineering. *J. Phys. Chem. Lett.* **2018**, *9*, 1243−1248.

(27) Engelhardt, G.; Cao, J. Dynamical Symmetries and Symmetry-Protected Selection Rules in Periodically Driven Quantum Systems. *Phys. Rev. Lett.* **2021**, *126*, 090601.

(28) Yan, Y. J. Theory of open quantum systems with bath of electrons and phonons and spins: Many-dissipaton density matrixes approach. *J. Chem. Phys.* **2014**, *140*, 054105.

(29) Tanimura, Y. Nonperturbative expansion method for a quantum system coupled to a harmonic-oscillator bath. *Phys. Rev. A* **1990**, *41*, 6676−87.
(30) Tanimura, Y. Stochastic Liouville, Langevin, Fokker-Planck, and master equation approaches to quantum dissipative systems. *J. Phys. Soc. Jpn.* **2006**, *75*, 082001.
(31) Yan, Y. A.; Yang, F.; Liu, Y.; Shao, J. S. Hierarchical approach based on stochastic decoupling to dissipative systems. *Chem. Phys. Lett.* **2004**, *395*, 216−21.
(32) Xu, R. X.; Cui, P.; Li, X. Q.; Mo, Y.; Yan, Y. J. Exact quantum master equation via the calculus on path integrals. *J. Chem. Phys.* **2005**, *122*, 041103.
(33) Xu, R. X.; Yan, Y. J. Dynamics of quantum dissipation systems interacting with bosonic canonical bath: Hierarchical equations of motion approach. *Phys. Rev. E* **2007**, *75*, 031107.
(34) Jin, J. S.; Zheng, X.; Yan, Y. J. Exact dynamics of dissipative electronic systems and quantum transport: Hierarchical equations of motion approach. *J. Chem. Phys.* **2008**, *128*, 234703.
(35) Zhang, H. D.; Xu, R. X.; Zheng, X.; Yan, Y. J. Nonperturbative spin-boson and spin-spin dynamics and nonlinear Fano interferences: A unified dissipaton theory based study. *J. Chem. Phys.* **2015**, *142*, 024112.
(36) Zhang, H. D.; Xu, R. X.; Zheng, X.; Yan, Y. J. Statistical quasi-particle theory for open quantum systems. *Mol. Phys.* **2018**, *116*, 780−812. Special Issue, "Molecular Physics in China".
(37) Wang, Y.; Xu, R. X.; Yan, Y. J. Entangled system-and-environment dynamics: Phase-space dissipaton theory. *J. Chem. Phys.* **2020**, *152*, 041102.
(38) Zhang, H. D.; Qiao, Q.; Xu, R. X.; Yan, Y. J. Effects of Herzberg-Teller vibronic coupling on coherent excitation energy transfer. *J. Chem. Phys.* **2016**, *145*, 204109.
(39) Weiss, U. *Quantum Dissipative Systems*; 3rd ed.; Series in Modern Condensed Matter Physics, Vol. *13*; World Scientific: Singapore, 2008.
(40) Kleinert, H. *Path Integrals in Quantum Mechanics, Statistics, Polymer Physics, and Financial Markets*, 5th ed.; World Scientific: Singapore, 2009.
(41) Yan, Y. J.; Xu, R. X. Quantum mechanics of dissipative systems. *Annu. Rev. Phys. Chem.* **2005**, *56*, 187−219.
(42) Hu, J.; Xu, R. X.; Yan, Y. J. Padé spectrum decomposition of Fermi function and Bose function. *J. Chem. Phys.* **2010**, *133*, 101106.
(43) Hu, J.; Luo, M.; Jiang, F.; Xu, R. X.; Yan, Y. J. Padé spectrum decompositions of quantum distribution functions and optimal hierarchial equations of motion construction for quantum open systems. *J. Chem. Phys.* **2011**, *134*, 244106.
(44) Yan, Y. J.; Jin, J. S.; Xu, R. X.; Zheng, X. Dissipaton equation of motion approach to open quantum systems. *Frontiers Phys.* **2016**, *11*, 110306.
(45) Tanimura, Y.; Kubo, R. Time evolution of a quantum system in contact with a nearly Gaussian-Markovian noise bath. *J. Phys. Soc. Jpn.* **1989**, *58*, 101−114.

https://doi.org/10.1021/acs.jpca.2c03308
J. Phys. Chem. A 2022, 126, 4554−4561